Composite Structures 160 (2017) 1119–1125

Contents lists available at ScienceDirect

Composite Structures

journal homepage: www.elsevier.com/locate/compstruct

Bilinear softening model and double *K* fracture criterion for quasi-brittle fracture of pultruded FRP composites

Wen Liu [a,b,*], Peng Feng [b], Jiankun Huang [a]

[a] Department of Civil Engineering, Beijing Forestry University, 100083 Beijing, PR China
[b] Department of Civil Engineering, Tsinghua University, 100084 Beijing, PR China

ARTICLE INFO

Article history:
Received 7 September 2016
Accepted 18 October 2016
Available online 5 November 2016

Keywords:
Pultruded FRP composites
Quasi-brittle fracture
Bilinear softening model
Double *K* fracture criterion
Cohesive fracture toughness

ABSTRACT

This study presents an experimental study on the mode I fracture property of pultruded fiber reinforced polymer (FRP) composites along the fiber direction. A quasi-brittle fracture exists for this material. The bilinear softening model is used to describe the constitutive relation in the cohesive fracture zone. Furthermore, a double *K* fracture criterion is applied to analyze the crack propagation and fracture property. The orthotropic effect on the fracture property of mode I along the fiber direction is rather small and ignored in this study. According to the bilinear softening model, the cohesive fracture energy is divided into two parts, the microcracking fracture energy and the fiber bridging fracture energy. The ratio between the two fracture energies and the model parameters are decided with the test results. For the double *K* fracture criterion, a cohesive fracture toughness in introduced to calculated the initial cracking fracture toughness. Based on the linear elastic fracture mechanics and the bilinear softening relation, the two fracture toughness of this criterion are obtained with the test results.

1. Introduction

Pultruded fiber reinforced polymer (FRP) composites is widely used in many structural applications. This material is usually thicker than other laminated FRP composites. Compared with traditional structural materials, such as concrete, steel, etc., it has the advantages of high strength and stiffness, high strength/weight ratio, resistance to certain corrosive environments, superior ability of energy absorption, and shielding ability in electrical or magnetic fields [1]. In recent decades, it has been widely used in the engineering. However, some manufacturing defects are produced during the production process of pultruded FRP, such as matrix microcracks and voids, which would form macrocracks and furthermore cause catastrophic failure [2]. As a result, traditional strength design theory is not adequate to evaluate the safety of this material. Fracture mechanics would be introduced to study its fracture property.

The fracture theory of FRP composites is rather complicated because of the anisotropic character and fiber reinforcing effect of this material. Most previous investigations focused on the unidirectional FRP laminated composites with thin cross section. For example, Sih et al. proposed a failure criterion of strain energy density to predict the fracture failure in unidirectional FRP composites subject to off-axis loading [3]. Armanios researched the interlaminar fracture of graphite/epoxy composites using a cracked-lap-shear configuration. A damage growth model was introduced to predict the fracture behavior [4]. Through the research on carbon fiber composites (CFRP) of mode I, mode II and mixed mode fracture, Ivens et al. found that the initiating interlaminar fracture toughness developed with the fiber surface treatment level [5]. Furthermore, a micromechanical model was built to explain how the interface fracture toughness influenced the initiating fracture toughness [6]. Ni et al. Studied the intralaminar fracture mechanism of three typical CFRP [7,8]. According to their research, the bridging fibers had an important effect on the intralaminar fracture toughness. The increment of the intralaminar fracture toughness was estimated on base of the adhesive force model. Rikards et al. investigated the mode I, mode II and mixed mode I/II interlaminar fracture properties of laminated glass fiber reinforced composites (GFRP) through a compact tensile test [9,10]. In the research, a fracture criterion was introduced, and the parameters were obtained by the finite element method as well as the modified virtual crack closure integral method. Brunner et al. reviewed the former criteria available for the interlaminar fracture of FRP, researched the delamination resistance of this laminated material,

* Corresponding author at: Department of Civil Engineering, Beijing Forestry University, 100083 Beijing, PR China.

E-mail address: liuwen@bjfu.edu.cn (W. Liu).

http://dx.doi.org/10.1016/j.compstruct.2016.10.134
0263-8223/

and introduced some models to calculated the fracture toughness [11–16].

On the other side, the fracture properties of thick-section pultruded FRP composites were also studied to model the fracture failure caused by the crack-like flaws. Haj-Ali et al. conducted some analytical and experimental studies on the mode I and mode II fracture properties of pultruded GFRP [1,2,17–21]. A nonlinear fracture analysis framework was developed, meanwhile, calibrated cohesive models were built to predict the crack growth for various crack geometries. Furthermore, a polynomial failure criterion of mixed fracture mode was introduced, also verified by the test results. According to former research, the most efficient theory way to analyze the fracture property of pultruded FRP was to build the cohesive zone model [22–24].

In this study, the mode I fracture property of pultruded FRP along the fiber direction is investigated. A bilinear model is applied to describe the constitutive relation in the cohesive fracture zone. Then a double K fracture criteria is introduced to explain the crack propagation and fracture process and. All the parameters are obtained by the test results of a three point fracture experiment on single edge notched (SEN) specimens.

2. Cohesive zone model

2.1. Bilinear softening relation

In the cohesive zone, it is supposed that the fracture process of mode I can be described by a fictitious crack which transferring the normal stress, σ. The classical bilinear softening model, which is widely used in fracture mechanics, is used to as the cohesive zone model in this study. As is shown in Fig. 1, the normal stress is calculated by the crack opening displacement (COD), w [25,26]. The cohesive zone begins to develop when the normal stress reaches its maximum value, i.e. its tensile stress, f_t. Then due to the fracture crack, the normal stress decreases with the increasing of COD. When the normal stress drops to zero, COD would reach its maximum value, w_c. With the parameters of the intersection point of the two lines, σ_s and w_s, this constitutive bilinear relation can be expressed as follows,

$$\sigma = \begin{cases} f_t - (f_t - \sigma_5)\frac{W}{W_S} & 0 \leqslant w < w_s \\ \frac{\sigma_5(w_c - w)}{w_c - w_s} & w_s < w < w_c \\ 0 & w = w_c \end{cases} \tag{1}$$

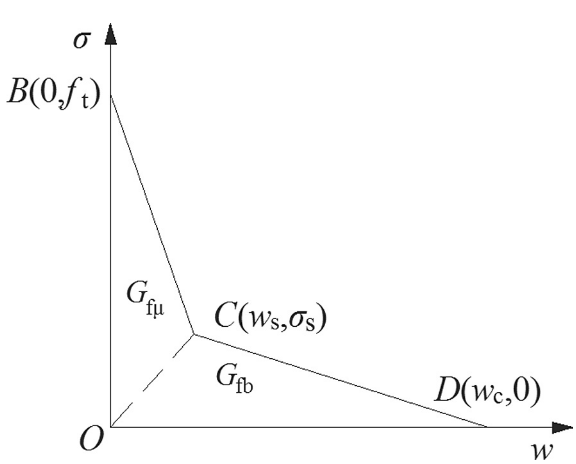

Fig. 1. Bilinear softening diagram.

The area under the entire curve, $f(w)$, is usually called the cohesive fracture energy, G_f. The value of this fracture energy is decided by four parameters, f_t, w_c, σ_s and w_s. The tensile stress, f_t, can be easily obtained by tensile tests, while the other three parameters are decided by fracture tests. From Fig. 1, it is seen that the cohesive fracture energy can be divided into two parts, the microcracking fracture energy, $G_{f\mu}$, and the crack bridging energy, G_{fb}, i.e. $G_f = G_{f\mu} + G_{fb}$. With the two fracture energies, $G_{f\mu}$ and G_{fb}, the values (w_s, σ_s) of the crossing point C can be calculated by an undimensional parameter $G_{f\mu}/G_f$. The parameters G_f, $G_{f\mu}/G_f$, and w_c in the cohesive fracture zone are studied by a simulation performed on SEN beams of thick-section pultruded FRP composites.

As a kind of orthotropic material, the model parameters pultruded FRP is different with isotropic material, such as concrete. In order to estimate the effect of orthotropy on the stress intensity factor of the orthotropic material of mode I fracture, Beom et al. calculated the stress intensity factor of cubic symmetry materials and evaluated the stress intensity factors of orthotropic materials by finite element analysis method [27]. According to the research, for the degenerate orthotropic material, the stress intensity factors depend very weakly on the material orthotropy when the crack angle is small. However, in this study, the crack is along the fiber direction, so the angle is zero. As a result, the effect of material orthotropy on the fracture property along the fiber direction is ignored, and linear elastic fracture mechanics is used to analyses the fracture property of pultruded FRP. Moreover, as another typical anisotropic material, the fracture property of wood is very similar to that of pultruded FRP. The longitudinal fracture property and the cohesive zone constitutive relationship of wood have been vastly researched before [28–31]. The results showed that the bilinear constitutive relation was suitable for its longitudinal fracture, and the model parameters were calculated with modeling and experiment methods.

2.2. Double K fracture criteria

It is supposed that the quasi-brittle fracture happens for pultruded FRP along the longitudinal direction, and a double K fracture criterion on base of linear elastic fracture mechanics, which is proposed for concrete fracture [32,33], is used to describe its crack propagation and fracture property. This fracture criteria is proved to be applicable for the longitudinal fracture of wood [34]. Here K means the fracture toughness. The double K parameters include the initial cracking fracture toughness, $K_{\rm I}^{\rm ini}$, and the failure fracture toughness, $K_{\rm I}^{\rm un}$. In the cohesive zone, the fracture crack develops in three stages: initial cracking, stable development, failure development. The corresponding fracture criteria is that, when $K < K_{\rm I}^{\rm ini}$, no crack appears; when $K_{\rm I}^{\rm ini} \leqslant K < K_{\rm I}^{\rm un}$, the crack develops stably; and when $K \geqslant K_{\rm I}^{\rm un}$, the crack develops unstably, the specimen is in the failure stage. The applied load P and the crack length a is used to determine $K_{\rm I}^{\rm ini}$ and $K_{\rm I}^{\rm un}$ according to the Stress Analysis of Cracks Handbook [35]. However, it is difficult to measure the initial cracking load in the test. Then in order to obtain an accurate initial cracking fracture toughness, a cohesive fracture toughness, $K_{\rm I}^{\rm c}$, and an elastic equivalent fictitious crack length, Δa_c, are introduced. The following relations exist for these parameters.

$$K_{\rm I}^{\rm ini} = K_{\rm I}^{\rm un} + K_{\rm I}^{\rm c} \tag{2}$$

$$\Delta a_c = a_c - a_0 \tag{3}$$

Where, a_c and a_0 represent the critical equivalent crack length and the initial crack length, respectively. The failure fracture toughness can be obtained with the test data, while the cohesive fracture toughness is calculated by the numerical integral method. Then the initial fracture toughness is determined according to Eq. (2).

3. Fracture experiment

3.1. Specimen preparation and test setup

A fracture experiment on pultruded GFRP is taken out in this study. As is shown in Fig. 2, three-point flexural test of mode I fracture is adopted according to the Stress Analysis of Cracks Handbook [35]. The specimen geometry is $l \times d \times b = 220\ \text{mm} \times 50\ \text{mm} \times 18\ \text{mm}$, with a support span s as 200 mm. The ratio of span to height is determined as $s/d = 4$. A single edge notch along the fiber direction is cut with the thickness of 2 mm, while the notch tip is made with a thickness as 0.5 mm. The notch depth a_0 is determined to be 15 mm, the ratio of notch depth to specimen height is $a_0/d = 0.3$.

The tests are conducted on a 10-kN electron-mechanical testing machine. As is shown in Fig. 2, a longitudinal load P is applied along the fiber direction, in the same line with the notch. Displacement control is used with a constant rate of 0.1 mm/min. The test setup is shown in Fig. 3. Two clip gauges with a measuring range of ±2 mm attached to the specimen are used to measure the crack mouth opening displacement (CMOD) and the crack tip opening displacement (CTOD). Moreover, another clip gauge with a measuring range of ±10 mm is used to measure the midspan deflection. In order to measure the initial cracking load, one half bridge and one full bridge with three strain gauge of are pasted in front of the notch tip.

3.2. Experiment result

Fig. 4 shows the experimental curves of P-CMOD and P-CTOD. From these two diagrams, a quasi-brittle fracture of mode I happens for pultruded FRP along the fiber direction. The P-CMOD and P-CTOD curves both include three stages in consistent with the crack growth. In the first stage, no crack develops in the specimen, and a liner relation exists for the curves. In the second stage, the crack grows stably, and a fracture process zone develops. In the third stage, the crack grows rapidly, leading to the fracture failure of the specimen. A typical plot of P-CMOD curve is sown in Fig. 5, in which, the three stages, OA, AB and BC, are marked. In stage OA, a linear elastic relation exhibit between the applied load and the specimen displacement. Then, in stage AB, because of the crack weakening effect, a strain softening relation happens. In stage BC, due to the effect of fibers, the specimen would not break into two parts immediately after cracking. Instead, the displacements develop slowly with a decline of the applied load. The two dividing points, A and B, represent the initial cracking point and the maximum load point respectively.

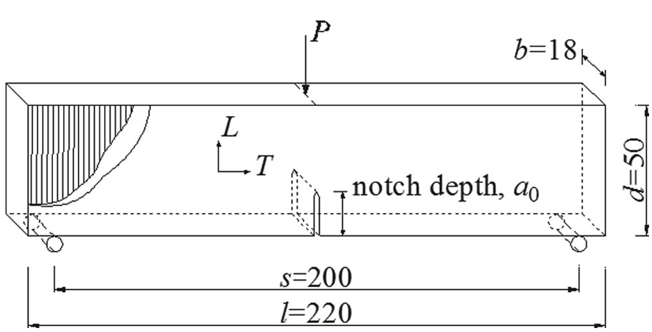

Fig. 2. Specimen geometry/mm.

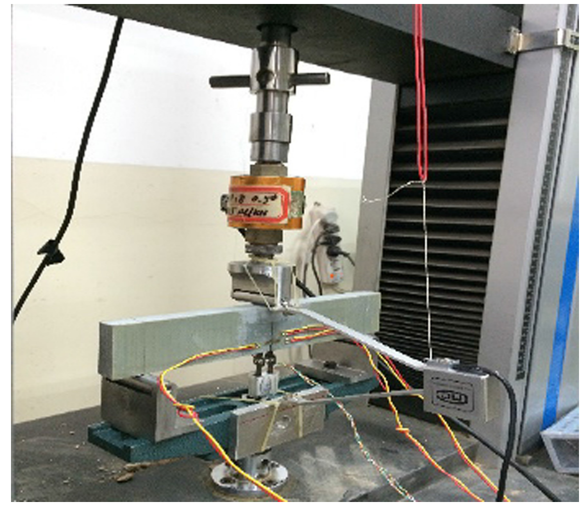

Fig. 3. Test setup.

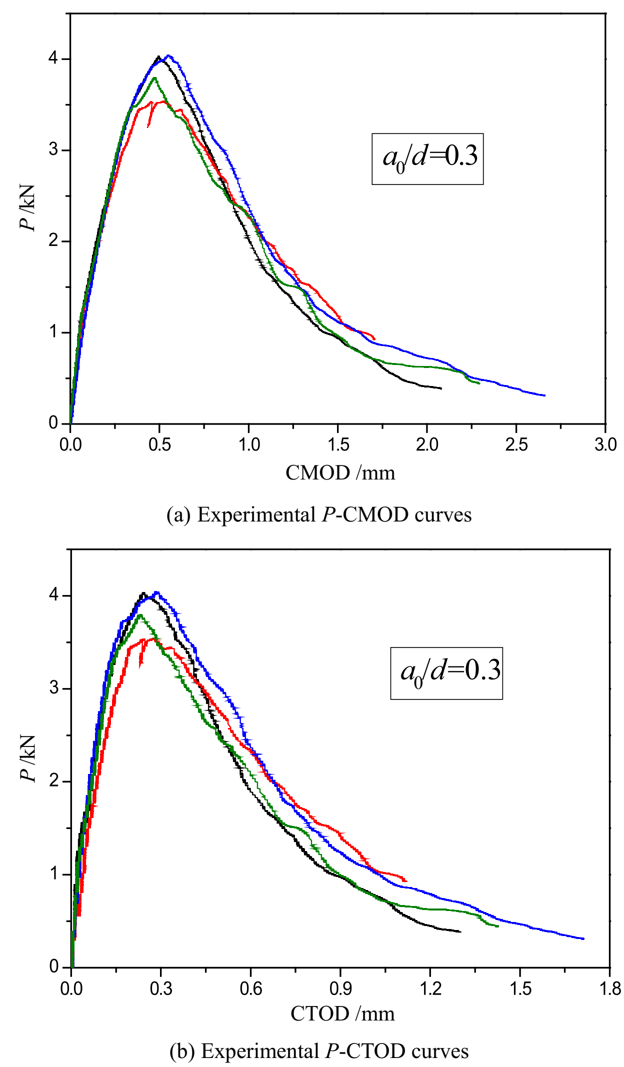

Fig. 4. Experimental P-CMOD and P-CTOD curves.

Fig. 6 shows a typical failure section of the fracture specimen, which is amplified by 700 times. It is seen that the fracture crack first destroys the bonding interfaces between the glass fiber and

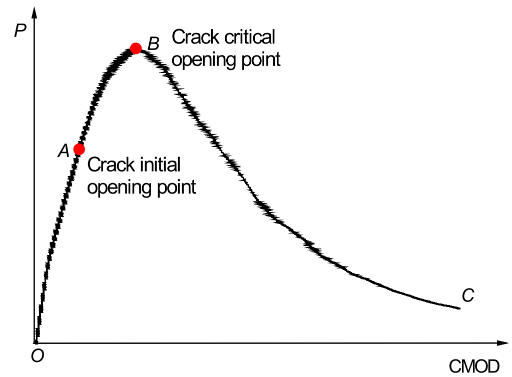

Fig. 5. Schematic plot of *P*-CMOD curve.

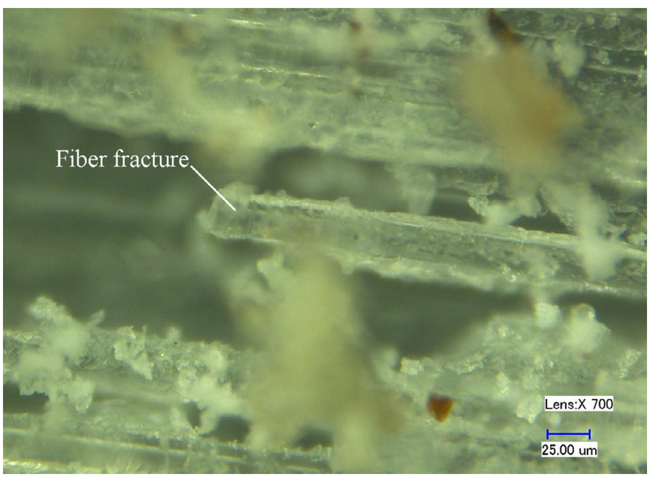

Fig. 6. Amplified cracking section.

the matrix, and then causes fiber fracture. More and more fibers continue to break, meanwhile, the matrix is also damaged on this cracking section. While the fracture develops to the top surface, the specimen reaches the final failure point.

4. Double *K* fracture criteria

4.1. Bilinear softening model parameters

From the above discussion of Eq. (1), it is very important to decide the values of the three parameters, w_c, σ_s and w_s. These parameters can be calculated with the total fracture energy G_f, and its two component parts, $G_{f\mu}$ and G_{fb}. According to the former research, linear elastic fracture mechanics (LEFM) can be used to obtain the fracture energy of wood, which is a another typical three anisotropic material [28,36], very similar to pultruded FRP. In this study, the method of LEFM is employed to calculate the fracture energy of pultruded FRP.

During the process of crack propagation and stress development in the cohesive zone after the initial cracking, the development of the cohesive zone can be divided into two stages [28,36]. In the first stage, the initial crack develops slowly due to the bridging effect of the glass fibers and the bonding effect of the matrix. The crack does not develop thoroughly in the cohesive zone, meaning that the applied load can steadily increase although a fracture crack has been produced. Then in the second stage, after the crack reaches its critical length, the matrix in the cohesive zone is thoroughly passed, and the crack develops rapidly, leading to the decrease of the applied load. The dividing point of the two stages is the critical crack length a_c, which corresponds to the maximum load P_{max} (point B in Fig. 5). While the starting point of the first stage is initial cracking point (point A in Fig. 5).

As is seen in Fig.1, the total fracture energy is defined as the area under the stress-displacement curve for the specimen, as follows,

$$G_f = \int_0^{w_c} \sigma \mathrm{d}w \tag{4}$$

In another way, for SEN bending specimen, the total fracture energy can be calculated as the work summation performed by the applied load and the self weight of the test piece, relative to the area of the fractured surface, as follows,

$$G_f = \frac{1}{S}\left(mg \cdot \delta_0 + \int_0^{\delta_0} P\mathrm{d}\delta\right) \tag{5}$$

Where, δ_0 is the mid-span deflection recorded from the start to the complete fracture, S represents theoretical (nominal) fractured ligament area, mg is the self-weight of the test specimen, and P is the applied load recorded during the fracture test. However, because that the work of self-weight is usually rather small in comparing with that of the applied force, the first part in Eq. (5) is ignored in computing the fracture energy, that is,

$$G_f = \frac{1}{S}\int_0^{\delta_0} P\mathrm{d}\delta = \frac{\int_0^{\delta_0} P\mathrm{d}\delta}{b(d-a_0)} \tag{6}$$

The fracture energy G_f is calculated with the experimental P-δ curves of the test specimens, which are shown in Fig. 7. The two component parts also can be calculated, in that, the microcracking fracture energy $G_{f\mu}$ is the area under the P-δ curve before the point of maximum applied load, while the crack bridging energy G_{fb} is the other part after the point of maximum load. With the experimental data, the calculated results of the three kinds of fracture energy are shown in Table 1. From this table, the unidimensional parameter $G_{f\mu}/G_f$ is a stable value for the specimens in this study. Here, it is taken as $G_{f\mu} = 0.6G_f$. With this value as well as the tensile strength f_t, the parameter w_s is easily calculated. In order to decide the other two parameters σ_s and w_c, the ratio value of w_s/w_c must be determined according to the softening σ-w relation. From the P-CMOD and P-CTOD curves shown in Fig. 4, w_s/w_c is set as 0.11. With these relations, the parameters in Eq. (1) are easily deduced, and all can be calculated with the fracture energy G_f and the tensile strength f_t, as shown in Eq. (6).

From the above discussion, the parameters of the bilinear softening relation of pultruded FRP composites is decided as shown in

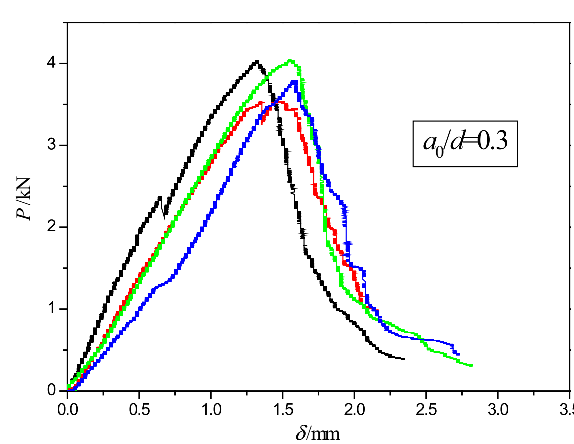

Fig. 7. Experimental P-δ curves.

Table 1
Calculated results of fracture energy.

Specimen	G_f (kJ/m^2)	$G_{f\mu}$ (kJ/m^2)	G_{fb} (kJ/m^2)	$\beta = G_{f\mu}/G_f$
No. 1	7.711	4.562	3.149	0.592
No. 2	7.543	4.467	3.076	0.592
No. 3	8.294	5.173	3.121	0.624
No. 3	7.530	4.554	2.976	0.605
Average	7.767	4.680	3.081	0.603

Eq. (7), while the tensile strength f_t is obtained through the direct tensile test, and the result is 36.76 MPa. A comparison of the calculated w_s by Eq. (7) and the tested $CTOD_c$ for each specimen is taken out, as is shown in Table 2. Here, $CTOD_c$ means the critical value of the crack tip opening displacement at the maximum applied load. In the fracture experiment, $CTOD_c$ is difficult to measure accurately by the clip gauge. However, in the bilinear relation, $CTOD_c$ is the crossing value of the crack opening displacement of the two lines, that is w_s. From Table 2, the difference error is computed as $e_1 = (|w_s - CTOD_c|/w_s)$. It is seen that the error between the calculated w_s and the tested $CTOD_c$ is not very big.

$$\begin{cases} \sigma_s = \frac{f_t}{14} \\ w_s = \frac{1.2G_f}{f_t} \\ w_c = \frac{11.2G_f}{f_t} \end{cases} \tag{7}$$

4.2. Double K fracture parameters

As illustrated in 2.1, the effect of orthotropy is ignored in calculate pultruded FPR's fracture toughness of mode I along the fiber direction. The Double *K* fracture criterion is applied to express the fracture property of pultruded FRP.

According to the Stress Analysis of Cracks Handbook [35], the following relation between the applied load *P* and CMOD exists for the thee point flexural fracture beam when $s/d = 4$.

$$\begin{aligned} \mathrm{CMOD} &= \frac{24Pa}{bdE}V_1(a/d) \\ V_1(a/d) &= 0.76 - 2.28a/d + 3.87(a/d)^2 - 2.04(a/d)^3 + \frac{0.66}{(1-a/d)^2} \end{aligned} \tag{8}$$

Based on this equation, for each specimen, three values of the longitudinal elastic modulus of pultruded FRP are calculated with three points in the linear stage of the *P*-CMOD curve. Then the longitudinal elastic modulus is determined as the mean value of the three calculated elastic modulus values.

In the typical P-CMOD curve showed in Fig. 5, points A and B represent the maximum elastic point and the maximum load point respectively. Before point A, the crack does not propagate, with a constant length a_0. The applied load at point A, is the initial cracking load P_{ini}. With P_{ini} and a_0, the initial cracking fracture toughness K_I^{ini} is calculated by Eq. (9) on basis of the elastic fracture mechanics. However, in fact, this value is difficult to obtain exactly with the test data, because that P_{ini} is difficult to examine accurately in the experiment.

Table 2
Comparison between the calculated w_s and the tested $CTOD_c$.

Specimen	w_s/mm	$CTOD_c$/mm	e_1/%
No. 1	0.252	0.238	5.56
No. 2	0.246	0.271	10.16
No. 3	0.271	0.287	5.90
No. 3	0249	0.230	7.63
Average	0.255	0.257	–

$$\begin{aligned} K_I^{ini} &= \frac{3P_{ini}s}{2bd^2}F_2(a_0/d) \\ F_2(a_0/d) &= \frac{1.99-(a_0/d)(1-a_0/d)[2.15-3.93a_0/d+2.7(a_0/d)^2]}{(1+2a_0/d)(1-a_0/d)^{3/2}} \end{aligned} \tag{9}$$

The failure fracture toughness K_I^{un} is calculated with the test data of the beginning point or the failure stage, which is point B in Fig. 5. With P_{max} and a_c, the failure fracture toughness K_I^{un} is computed also by Eq. (9), with substituting P_{max} and a_c for P_{ini} and a_0 respectively. However, it is difficult to measure a_c in the experiment. In this research, the linear superposition assumption is used to obtain a_c. There are two hypotheses in this theory: (1) the nonlinear part of *P*-CMOD curve is caused by the fictitious crack in the cohesive zone; (2) the effective crack contains two parts: equivalent elastic free crack and equivalent elastic fictitious crack. In this way, according to Eq. (8), the critical crack length a_c, is calculated with the maximum applied load P_{max}, the critical crack mouth opening displacement $CMOD_c$ corresponding to this maximum load, and the elastic modulus *E*.

From Eq. (3), when the failure fracture toughness K_I^{un} is obtained. the cohesive fracture toughness K_I^c, is used to calculate the initial cracking fracture toughness K_I^{ini}. Numerical integration method is used to determine the cohesive fracture toughness. According to the Stress Analysis of Cracks Handbook [35], for a limitless narrow plate under a couple of unit force, as shown in Fig. 8, the stress intensity factor at the crack tip is calculated as follows,

$$\begin{aligned} K_I &= \frac{2}{\sqrt{\pi a}}F_1\left(\frac{x}{a},\frac{a}{d}\right) \\ F_1\left(\frac{x}{a},\frac{a}{d}\right) &= \frac{3.52-\left(1-\frac{x}{a}\right)}{\left(1-\frac{a}{d}\right)^{3/2}} - \frac{4.35-5.28\frac{x}{a}}{\left(1-\frac{a}{d}\right)^{1/2}} + \left\{\frac{1.30-0.30\left(\frac{x}{a}\right)^{3/2}}{\left[1-\left(\frac{x}{a}\right)^2\right]^{1/2}} + 0.83 - 1.76\frac{x}{a}\right\} \\ &\quad \times\left[1-\left(1-\frac{x}{a}\right)\frac{a}{d}\right] \end{aligned} \tag{10}$$

where, *x* is the distance between a free point on the fracture crack and the bottom surface. When the applied load on the specimen reaches the maximum load P_{max}, the crack mouth opening displacement reaches its critical value, $CMOD_c$. The cohesive softening stress is distributed as shown in Fig. 8.

From Fig. 8, the cohesive softening stress at the free point on the fracture crack is calculated as follows,

$$\sigma(x) = \sigma_s(CTOD_c) + \frac{x-a_0}{a-a_0}[f_t - \sigma_s(CTOD_c)] \tag{11}$$

This equation is transferred into,

$$\sigma\left(\frac{x}{a}\right) = \sigma_s(CTOD_c) + \frac{\frac{x}{a}-\frac{a_0}{a}}{1-\frac{a_0}{a}}[f_t - \sigma_s(CTOD_c)] \tag{12}$$

$0 \leqslant CTOD \leqslant CTOD_c$ or $a_0 \leqslant x \leqslant a_c$

where, $\sigma_s(CTOD_c)$ is the cohesive stress at the crack tip when the crack tip opening displacement reaches its critical value, $CTOD_c$. This stress is computed through the bilinear softening relation as shown in Eqs. (1) and (7), in which, $CTOD_c = w_s$. Then, with this cohesive stress, the stress intensity factor induced by the cohesive stress at the critical failure point is obtained, as shown in Eq. (13).

$$K_I^c = -\int_{a_0}^{a_c} \frac{2\sigma\left(\frac{x}{a_c}\right)}{\sqrt{\pi a_c}}F_1\left(\frac{x}{a_c},\frac{a_c}{d}\right)dx \tag{13}$$

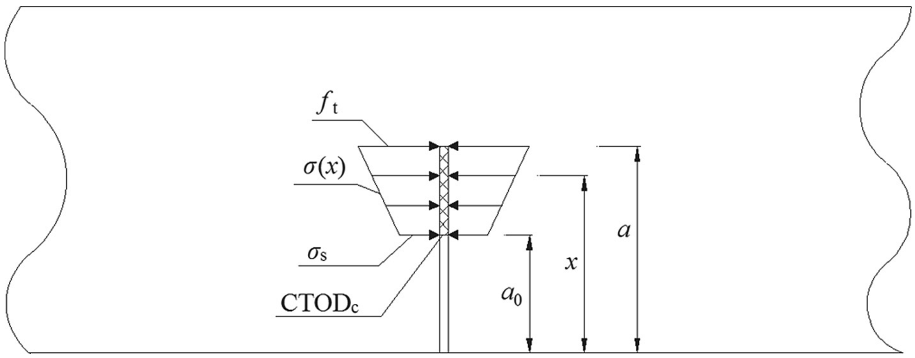

Fig. 8. Cohesive softening stress distribution at the maximum applied load.

Taking $V = \frac{a_c}{d}$, and $U = \frac{x}{a_c}$, then $dx = a_c dU$. Eq. (13) is fatherly transferred into

$$K_I^c = -\int_{a_0/a_c}^{1} 2\sqrt{\frac{a_c}{\pi}}\sigma(U)F_1(U,V)dU$$

$$F_1(U,V) = \frac{3.52-(1-U)}{(1-V)^{3/2}} - \frac{4.35-5.28U}{(1-V)^{1/2}} + \left[\frac{1.30-0.30U^{3/2}}{1-(1-U^2)^{1/2}} + 0.83 - 1.76U\right] \times [1-(1-U)V] \tag{14}$$

According to these above two equations, it is clearly that the two critical values, a_c and $CTOD_c$ are necessary to calculate K_I^c. From the above analysis, a_c can be obtained with P_{max}, $CMOD_c$ and E according to Eqs. (8) and (9), while $CTOD_c$ is determined as w_s in the bilinear softening model.

From the above discussion, the double K parameters can be obtained as follows, a. determine the elastic modulus E according to Eq. (9) with the experimental P-CMOD curve; b. calculate the critical equivalent crack length a_c with the maximum load P_{max}, the critical crack mouth opening displacement $CMOD_c$, and the elastic modulus E; c. calculate the critical crack tip opening displacement $CTOD_c$ by the bilinear softening relation; d. numerical integrate the cohesive fracture toughness K_I^c; f. calculate the failure fracture toughness K_I^{un} with the experimental data; e. calculate the initial cracking fracture toughness K_I^{ini} with K_I^{un} and K_I^c, then compare it with the experimental K_I^{ini}.

Following the above procedures, the experimental and calculated results of the specimens in this study are shown in Table 3. $\bar{K}_I^{ini}$ is the experimental initial cracking fracture toughness obtained from the a_0 and the tested P_{ini}, while K_I^{ini} represents the calculated value determined by K_I^{un} and K_I^c according to Eq. (3). The difference error e_2 is computed as $e_2 = (| \ K_I^{ini} - \bar{K}_I^{ini}/\bar{K}_I^{ini})$. From this table, the difference between the experimental and the calculated initial fracture toughness is rather apparent. It is better to determine this value with the cohesive fracture toughness. Moreover, the double K of the pultruded GFRP in this study is obtained as $K_I^{ini} = 0.$ MPa mm$^{1/2}$ and $K_I^{un} = 0.416$ MPa·mm$^{1/2}$.

5. Conclusion

This study presents a three-point fracture experiment of mode I along the fiber direction on pultruded FRP composites. A bilinear softening model is used to describe the constitutive relation of the cohesive fracture zone, while a double K fracture criterion is applied to analyze the crack propagation and fracture process of this material. Based on the linear elastic fracture mechanics, the model parameters are obtained from the experiment result. The following conclusions are obtained.

(1) A quasi-brittle fracture of mode I happens for pultruded FRP along the fiber direction. According to the crack development, three stages exist during the fracture process: no developing stage, stable developing stage and failure stage, with the points of initial cracking and maximum load as their dividing points.
(2) For pultruded FRP, the orthotropic effect on the fracture property of mode I along the fiber direction is rather small, and ignored in this study. The bilinear softening model is used to describe the constitutive relation of this material in the cohesive fracture zone. The cohesive fracture energy includes two parts: the microcracking fracture energy and the fiber bridging fracture energy. The ratio between the two fracture energies is 1.5.
(3) A double K fracture criterion is applied to explain the crack propagation and fracture property of pultruded FRP. The cohesive fracture toughness in introduced to determine the initial cracking fracture toughness. Based on the linear elastic fracture mechanics and the bilinear softening relation, the two fracture toughness of this criterion is calculated with the test results.

Acknowledgements

The authors gratefully acknowledge the financial supports provided by the National Natural Science Foundation of China

Table 3
The calculated results of FRP's fracture toughness.

Specimen	Experimental data					Calculated results						e_2/%
	P_{ini} /kN	P_{max} /kN	$CMOD_c$/mm	a_0/mm	$\bar{K}_I^{ini}$ /MPa mm$^{1/2}$	E/GPa	a_c/mm	$CTOD_c$/mm	K_I^c/MPa mm$^{1/2}$	K_I^{un}/MPa mm$^{1/2}$	K_I^{ini}/MPa mm$^{1/2}$	
No. 1	3.50	4.03	0.498	15	0.167	10.53	28.44	0.252	−0.224	0.425	0.201	16.92
No. 2	3.11	3.53	0.458	15	0.149	11.38	32.27	0.246	−0.279	0.453	0.174	14.37
No. 3	3.72	4.04	0.556	16	0.178	9.12	27.43	0.271	−0.197	0.397	0.200	18.50
No. 4	3.40	3.80	0.474	15	0.163	10.56	27.97	0249	−0.203	0.388	0.185	11.89
Average	3.34	3.79	0.477	15	0.164	10.82	29.56	0.248	−0.226	0.416	0.190	–

(Projects 51522807 and 51308046) and the Open Fund Project of State Key Laboratory of Coastal and Offshore Engineering of Dalian University of Technology – China (No. LP1516).

References

[1] Haj-Ali R, Kilic H. Nonlinear constitutive models for pultruded FRP composites. Mech Mater 2003;35:791–801.
[2] Haj-Ali R, El-Hajjar R. Crack propagation analysis of mode-I fracture in pultruded composites using micromechanical constitutive models. Mech Mater 2003;35:885–902.
[3] Sih GC, Chen EP, Huang SL, McQuillen EJ. Material characterization on the fracture of filament reinforced composites. J Compos Mater 1975;9:167–86.
[4] Armanios EA. Interlaminar fracture in graphite/epoxy composites. Key Eng Mater 1989;37:85–102.
[5] Albertsen H, Ivens J, Peters P, Wevers M, Verpoest I. Interlaminar fracture toughness of CFRP influenced by fibre surface treatment: Part 1: Experimental results. Compos Sci Technol 1995;54:133–45.
[6] Ivens J, Wevers M, Verpoest I, Albertsen P, Peters M. Interlaminar fracture toughness of CFRP influenced by fibre surface treatment: Part 2: modelling of the interface effect. Compos Sci Technol 1995;54(2):147–59.
[7] Wamoto M, Ni QQ, Fujiwara T, Kurashiki L. Intralaminar fracture mechanism in unidirectional CFRP composites: Part I: Intralaminar toughness and AE characteristics. Eng Fract Mech 1999;64:721–45.
[8] Wamoto M, Ni QQ, Fujiwara T, Kurashiki K. Intralaminar fracture mechanism in unidirectional CFRP composites: Part II: analysis. Eng Fract Mech 1999;64:747–64.
[9] Rikards R, Buchholz FG, Wang H, Bledzki AK, Korjakin A, Richiard HA. Investigation of mixed mode I/II interlaminar fracture toughness of laminated composites by using a CTS type specimen. Eng Fract Mech 1998;61:325–42.
[10] Rikards R. Interlaminar fracture behaviour of laminated composites. Comput Struct 2000;76:11–8.
[11] Brunner AJ. Experimental aspects of mode I and mode II fracture toughness testing of fiber-reinforced polymer-matrix composites. Comput Methods Appl Mech Eng 2000;185:161–72.
[12] Brunner AJ, Flueler P. Prospects in fracture mechanics of "engineering" laminates. Eng Fract Mech 2005;72:899–908.
[13] Brunner AJ, Blackman BRK, Williams JG. Calculating a damage parameter and bridging stress from G_{IC} delamination tests on fiber composites. Compos Sci Technol 2006;66:785–95.
[14] Blackman BRK, Brunner AJ, Williams JG. Mode II fracture testing of composites: a new look an old problem. Eng Fract Mech 2006;73:2443–55.
[15] Brunner AJ, Blackman BRK, Davies P. A status report on delamination resistance testing of polymer-matrix composites. Eng Fract Mech 2008;75:2779–94.
[16] Brunner AJ, Murphy N, Pinter G. Development of a standardized procedure for the characterization of interlaminar delamination propagation in advanced composites under fatigue mode I loading conditions. Eng Fract Mech 2009;76:2678–89.
[17] Haj-Ali R, El-Hajjar R, Muliana A. Cohesive fracture modeling of crack growth in thick-section composites. Eng Fract Mech 2006;73:2192–209.
[18] Kilic H, Haj-Ali R. Progressive damage and nonlinear analysis of pultruded composite structures. Compos B Eng 2003;34:235–50.
[19] El-Hajjar R, Haj-Ali R. Mode-I fracture testing of thick section FRP composites using ESE(T) specimen. Eng Fract Mech 2005;72:631–43.
[20] El-Hajjar R, Haj-Ali R. In-plane testing of thick-section pultruded FRP composites using a modified Arcan fixture. Compos B Eng 2004;35:421–8.
[21] Muliana A, Haj-Ali R. Nested nonlinear viscoelastic and micromechanical models for the analysis of pultruded composite materials and structures. Mech Mater 2004;36:1087–110.
[22] Elices M, Guinea GV, Gomez J, Planas J. The cohesive zone model: advantage, limitations and challenges. Eng Fract Mech 2002;69:137–63.
[23] Planas J, Elices M, Guinea GV, Gomez J, Cendon DA, Arbilla I. Generalizations and specializations of cohesive crack models. Eng Fract Mech 2003;70:1759–76.
[24] Christian GH, Bazant ZP. Cohesive crack, size effect, crack band and work-of-fracture models compared to comprehensive concrete fracture tests. Int J Fract 2014;187:133–43.
[25] Hillerborg A, Modeer M, Petersson PE. Analysis of crack formation and crack growth in concrete by means of fracture mechanics and finite elements. Cem Concr Res 1976;6:773–82.
[26] Guinea GV. Modelling the fracture of concrete: the cohesive crack. Mater Struct 1995;28:187–94.
[27] Beom HG, Cui CB, Jang HS. Application of an orthotropy rescaling method to edge cracks and kinked cracks in orthotropic two-dimensional solids. Int J Eng Sci 2012;51:14–31.
[28] Morel S, Lespine C, Coureau JL, Dourado N. Bilinear softening parameters and equivalent LEFM R-curve in quasibrittle failure. Int J Solids Struct 2010;47:837–50.
[29] Coureau JL, Morel S, Dourado N. Cohesive zone model and quasibrittle failure of wood: a new light on the adapted specimen geometries for fracture tests. Eng Fract Mech 2013;109:328–40.
[30] Coureau JL, Morel S, Gustafsson PJ. Influence of the fracture softening behaviour of wood on load-COD curve and *R*-curve. Mater Struct 2006;40:97–106.
[31] Morel S, Dourado N, Gerard V, Morals J. Wood: a quasibrittle material R-curve behavior and peak load evaluation. Int J Fract 2005;131:385–400.
[32] Xu SL, Reinhardt HW. Determination of double-K criterion for crack propagation in quasi-brittle fracture, Part I: experimental investigation of crack propagation. Int J Fract 1999;98:111–49.
[33] Xu SL, Reinhardt HW. Determination of double-K criterion for crack propagation in quasi-brittle fracture, Part II: analytical evaluating and practical measuring methods for three-point bending notched beams. Int J Fract 1999;98:151–77.
[34] Xu SL, Reinhardt HW, Gappoev M. Mode II fracture testing method for highly orthotropic materials like wood. Int J Fract 1995;75:185–214.
[35] Tada H, Paris PC, Irwin GR. The Stress Analysis of Cracks Handbook. New York: ASME Press; 2000.
[36] Bostrom L. The stress-displacement relation of wood perpendicular to the grain, 1. Experimental determination of the stress-displacement relation. Wood Sci Technol 1994;28:309–17.